Applied Catalysis B: Environmental 310 (2022) 121345

Contents lists available at ScienceDirect

Applied Catalysis B: Environmental

journal homepage: www.elsevier.com/locate/apcatb

A comparison of SMX degradation by persulfate activated with different nanocarbons: Kinetics, transformation pathways, and toxicity

Yanhua Peng [a], Guansheng Xie [a], Penghui Shao [a,*], Wei Ren [a], Mengling Li [a], Yufeng Hu [b], Liming Yang [a], Hui Shi [a], Xubiao Luo [a,*]

[a] Key Laboratory of Jiangxi Province for Persistent Pollutants Control and Resources Recycle, Nanchang Hangkong University, Nanchang 330063, PR China
[b] School of Environmental and Municipal Engineering, North China University of Water Resources and Electric Power, Zhengzhou 450046, PR China

ARTICLE INFO

Keywords:
Persulfate
Carbon nanotubes
Nanodiamond
Toxicity
Degradation pathways

ABSTRACT

Nanocarbon-based advanced oxidation processes (AOPs) are widely used in wastewater purification. However, the properties of different carbon catalysts lead to differences in the organic degradation mechanism and toxicity of wastewater treatment. Herein, this study provides insight into the differences between the oxidation of sulfamethoxazole (SMX) by carbon nanotube (CNT)/peroxymonosulfate (PMS), nanodiamond (ND)/PMS and PMS-alone systems. The pseudo-first-order reaction constant of the reaction of the $SO_4^{\bullet-}$-dominated CNT/PMS system with SMX is 19-fold and 30-fold higher than those of the $^1O_2$-dominated ND/PMS system and PMS direct oxidation system at pH= 7, respectively. In addition, density functional theory (DFT) calculations and product analysis show that $SO_4^{\bullet-}$ mainly attacks the aniline and sulfonyl groups, while oxidation of the aniline group is the dominant mode of PMS direct oxidation and $^1O_2$ reactivity. The formation of nitro and nitroso byproducts after SMX degradation determines the toxicity difference, and the CNT/PMS system is even more advantageous.

1. Introduction

Sulfamethoxazole (SMX) is an important antibiotic that has been widely used to treat diseases and infections. However, most SMX is not absorbed into the body and is instead excreted unaltered into sewage systems, leading to toxic effects on aquatic ecosystems and humans [1–3]. The annual use of antibiotics worldwide has been reported to range from 100,000 to 200,000 tons, of which 50–75% are used in veterinary prophylaxis as growth promoters in animal breeding [4]. The proportion of sulfonamides used in veterinary antibiotics ranges from 2% (US) to 22% (UK, Kenya) in different countries. Sulfonamides at concentrations below lethal levels also pose a serious risk to health and the environment, as pathogenic bacteria develop resistance to these compounds and disinfection products, and they can poison humans if their concentrations exceed the safe limits [5,6]. Therefore, the use of wastewater treatment technologies, such as physical adsorption, photocatalysis, biodegradation and chemical oxidation, is of great significance in controlling environmental organic pollutants in actual wastewater [7–9].

Nanocarbon-based advanced oxidation processes (AOPs) are promising technologies for the elimination of antibiotics in water. Various carbon nanomaterials have been proven to be excellent candidates for the activation of persulfate and to serve as catalysts for green remediation technologies. Nanocarbon persulfate has highly efficient SMX degradation activity, and more importantly, it can reduce the toxicity of SMX degradation products [10–12]. The reasons for the decrease in toxicity are attributed to (i) the adsorption of SMX by nanocarbon-based materials; (ii) the strong oxidation capacity of generated reactive oxygen species (ROS); and (iii) the special physical and chemical properties of carbon nanomaterials. Many kinds of carbon-based nanomaterials have been applied in persulfate-based AOPs, including CNT, ND, graphene, carbon dots and mesoporous carbon [13]. However, their physical and chemical properties are very different, resulting in uneven catalytic performance and different activation mechanisms of persulfate [14,15]. For example, N-doped CNT were reported to activate persulfate for the oxidation of phenol through a nonradical pathway [16]. Graphitized ND can mediate electron transfer from phenol to persulfate by forming charge-transfer complexes, thus exhibiting excellent performance in phenol oxidation [17]. CNT and ND are two classical carbon nanomaterials that are excellent catalysts for persulfate activation due to their unique biocompatibility and relatively high thermal stability [18]. Currently, carbonaceous nanomaterials and nanocomposites are widely

* Corresponding authors.
E-mail addresses: penghui_shao@163.com (P. Shao), luoxubiao@126.com (X. Luo).

https://doi.org/10.1016/j.apcatb.2022.121345
Received 15 February 2022; Received in revised form 18 March 2022; Accepted 20 March 2022
Available online 23 March 2022

used in various fields, and their morphology, electrochemical performance, and mechanical properties can be regulated, enabling environmental remediation [19–25].

CNT consist mainly of sp^2 carbon atoms. They have a simple structure, high carbon content and low oxygen content. The highly crystalline and conjugated π-network of CNT enables the generation of sulfate and hydroxyl radicals for phenol degradation [16]. In the activation process, peroxydisulfate (PDS) is activated on the CNT surface to form the metastable complex CNT-PDS* , and phenol is oxidized by CNT-PDS* via an electron-transfer process [26]. In addition, defects in CNT serve as important active sites. Defect-rich CNT show superior activity in peroxymonosulfate (PMS) activation, and organics are removed through a nonradical electron-transfer process [27]. In contrast, ND is a carbon material with an sp^3-hybridized structure, and its grain boundaries with unsaturated dangling bonds usually undergo obvious surface relaxation. The hybridization structure of ND can be regulated to promote its catalytic activity by controlling the heat treatment conditions; such treatment can effectively remove oxygen from the surface and lead to higher activity [28]. The sp^3-hybridized ND can be transformed into a uniform shell/core (sp^2/sp^3) hybrid or concentric graphite onion (sp^2), with its mechanism of persulfate activation ranging from radical to nonradical pathways. In the radical pathway, transient intermediates and water oxidation processes at the surface of the ND can activate PMS to generate sulfate radicals and hydroxyl radicals, and surface-attached sulfate radicals can degrade phenol [29]. In the nonradical pathway, the carbonyl groups on the surface of the ND are important active sites that can generate singlet oxygen for 4-chlorophenol removal by activating PMS [30,31]. In summary, the different mechanisms of persulfate activation on two noncarbon materials (CNT and ND) remain unclear, prompting evaluations of their organic substance removal and detoxification in wastewater treatment. Therefore, in this paper, CNT and ND were used as catalysts to activate PMS for SMX removal, and the oxidation mechanism was determined by chemical quenching, capture methods and electrochemical experiments. Key influencing factors, such as pH, inorganic ions and natural organic matter (NOM), were investigated during SMX degradation. Moreover, high-performance liquid chromatography (HPLC)/electrospray ionization tandem mass spectrometry (ESI-MS/MS) and toxicity tests were used to identify the conversion products of SMX and assess their toxicity. In addition, the electron density of each atom in the SMX structure was calculated using density functional theory (DFT) to study the oxidation pathways of SMX, and toxicity differences caused by the formation of nitro and nitro byproducts after SMX degradation were analyzed. Ultimately, the results indicated that the CNT/PMS system degraded the SMX more efficiently than the other studied systems, offering the possibility of practical application in wastewater treatment.

2. Materials and methods

2.1. Materials

Potassium peroxymonosulfate (PMS, $2KHSO_5{\cdot}3KHSO_4.3\ K_2SO_4$, available as Oxone), sodium phosphate monobasic monohydrate, sodium phosphate dibasic, 5,5-dimethyl-1-pyrrolidine, 2,2-azino-bis(3-ethylbenzothiazoline)− 6-sulfonic acid diammonium salt (ABTS) and *tert*-butyl alcohol (TBA) were purchased from Sigma–Aldrich. Sulfamethoxazole (SMX), sodium thiosulfate ($Na_2S_2O_3{\cdot}5\ H_2O$), and 2,2,6,6-tetramethyl-4-piperidone (TEMP) were purchased from J&K Scientific Co. HPLC-grade acetic acid was purchased from MREDA Technology Inc. (China). HPLC- or UPLC–MS-grade methanol and acetonitrile were purchased from Merck (USA). All the other chemicals were at least of analytical grade and used without further purification. All working solutions were prepared in 18.2 MΩ·cm Milli-Q water.

2.2. Preparation of the nanocarbon-based catalysts

Raw NDs (Sigma–Aldrich) were transferred to a quartz tube and annealed at 800 °C under an argon atmosphere for 2 h to obtain the final annealed ND. Raw multiwalled CNT (MWCNT, Sigma–Aldrich) were added to a mixed acid solution (3 mL HNO_3 and 9 mL H_2SO_4) at 75 °C for 6 h. Then, the pH of the mixed liquid was adjusted to neutral through the addition of a basic solution and water. The CNT were transferred to a quartz tube and annealed at 1000 °C under an argon atmosphere for 2 h to obtain the final annealed CNT.

2.3. Catalytic degradation experiment

Batch experiments were carried out in a series of 100 mL beakers containing 0.15 mM SMX at 25 ± 2 °C. The initial pH was adjusted to the desired values by 10 mM phosphate buffer. Reactions were initiated by spiking an appropriate amount of PMS stock solution (50 mM) into the beaker. Aliquots (1.5 mL) were withdrawn at predetermined time intervals, and each sample (0.5 mL) was spiked in HPLC vials that initially contained 200 μL 0.1 M $Na_2S_2O_3$ to quench the residual PMS. The samples were analyzed immediately. The remaining sample was transferred to a colorimetric tube to analyze the concentration of PMS by ultraviolet–visible (UV–VIS) spectrophotometry.

2.4. Analytical methods

The concentrations of SMX were determined on an HPLC 1525 system equipped with a Waters 717 autosampler and a Waters 2487 dual λ detector. A Waters symmetry C18 column (4.6 mm × 150 mm, 5 μm particle size) was used for separation. The concentrations of PMS were measured on an ABTS-based colorimetric method. An eluent of water and acetonitrile (60/40, v/v%) was used to separate the SMX and its products at a flow rate of 1.0 mL/min. The concentration of SMX was quantified at λ = 265 nm. To identify the oxidation products of SMX, a triple quadrupole time-of-flight (TOF) mass spectrometer (Waters Xevo G2 QTof) coupled with an ultraperformance liquid chromatography (UPLC) system was used. Chromatographic separations were performed using a Poroshell 120 EC-C18 column (50 mm × 3.0 mm, 2.7 μm). Accurate MS^E patterns of SMX and its oxidation products were analyzed in molecular ion scanning mode (m/z 50–1000) in positive ESI mode.

2.5. Natural water samples

Natural river water was sampled from the Ganjiang River, one of the main tributaries of the Yangtze River located in Jiangxi Province. Tap water was obtained from the municipal pipe network. The natural water samples were filtered through a 0.2 μm membrane filter and stored at 4 °C prior to use. The properties of the two natural water samples are provided in Table S1.

2.6. Toxicity analysis

The toxicity of the degradation products to aquatic organisms was investigated by using the green algae Chlorella sp. obtained from Nanchang Hangkong University. The detailed protocol for preparing the cultivation medium can be found in a previous study [32]. The growth rate was monitored in terms of the optical density (OD) at a wavelength of 680 nm. Additionally, the concentrations of chlorophyll A and chlorophyll B were measured with a microplate reader (SpectraMax M5) at wavelengths of 666 and 653 nm, respectively. The detailed analytical methods are provided in Supporting Information Text S1.

3. Results and discussion

3.1. Oxidative degradation of SMX

The activities of the three oxidation systems were evaluated by investigating the kinetics of SMX. As shown in Fig. 1a, the NDs exhibited poor SMX adsorption, and the removal rate reached 2.47% within 60 min. The CNT had superior SMX adsorption (15.33%) because the CNT had a larger surface area (297 m^2/g) than the NDs (133 m^2/g), resulting in sufficient active sites on the CNT surface to efficiently adsorb SMX (Fig. S1 and Table S2). PMS alone attained a 39.33% removal rate of SMX, suggesting that SMX can be directly oxidized by PMS in neutral or alkaline solutions [3]. The curves of PMS alone and PMS adsorbed onto CNT intersected at approximately 15 min because 15.33% of the SMX was rapidly adsorbed onto the CNT and reached equilibrium within 5 min, while the rate of PMS oxidation was slow with zero-order kinetics; 39.33% of the SMX was finally removed after 60 min. Once NDs and CNT were introduced into the PMS solution, the SMX removal rates were 55.01% and 99%, respectively, within 10 min, which were better than the removal efficiency observed in previous studies (Table S3). According to the calculated oxidation kinetics of SMX (Text S2), the kinetic constant of the CNT/PMS system was as high as 0.3008 min^{-1}, which was 19.79-fold and 30.85-fold higher than that of the systems containing ND/PMS (0.0152 min^{-1}) and PMS alone (0.00975 min^{-1}), respectively (Fig. S2). This result might have occurred because the specific surface area of the CNT (297 m^2/g) was larger than that of the NDs (133 m^2/g), which was beneficial to the mass transfer of reactants (PMS and SMX) from solution to the surface of the catalysts (CNT and ND). Hence, the CNT, which had a large specific surface area, could provide more active sites for PMS activation and SMX oxidation. Additionally, some ROS were generated in the ND/PMS and CNT/PMS systems. The consumption of PMS was monitored during the oxidation process (Fig. 1b). The PMS consumption rates of the systems with PMS alone, ND/PMS and CNT/PMS were 34.4%, 48.7% and 97.6%, respectively. The varying trend of PMS consumption was identical to the trend in the kinetic constant of SMX oxidation, which illustrates that CNT had higher performance than ND in the activation of PMS and oxidation of SMX.

3.2. Identification of ROS

3.2.1. EPR experiments

To study the evolution and identity of the ROS involved in the three systems, we used a range of techniques, such as free radical capture and visualization (by electron paramagnetic resonance (EPR) spectroscopy), selective ROS quenching, and online open-circuit potential monitoring, to identify free radical and nonradical processes. *In situ* EPR analysis was conducted with 5,5-dimethyl-1-pyrroline *N*-oxide (DMPO) (or TEMP) as a radical (or singlet oxygen, respectively) spin trapping agent. As shown in Fig. 2a, no significant signal was observed in the presence of PMS alone. A seven-line EPR signal was observed when DMPO was present in the CNT/PMS and ND/PMS systems, which was attributed to a DMPOX spin adduct [33]. DMPOX may be generated in two ways: oxidative attack of the complex and transition oxidation of sulfate radicals or singlet oxygen [34,35]. Moreover, Fig. 2b shows that the TEMP-$^1O_2$ signal was not observed with PMS alone or CNT/PMS but appeared in the spectrum of the ND/PMS system because C═O was the main active site on the ND surface that could activate PMS to produce $^1O_2$. The degradation of SMX by PMS is a direct oxidation process that generates $^1O_2$, and the absence of $^1O_2$ in the CNT/PMS system may be because the CNT surface with its sp^3 hybrid structure has a lower carbonyl content. Therefore, the main ROS of the CNT/PMS and ND/PMS systems might be sulfate radicals and singlet oxygen, respectively.

3.2.2. Chemical quenching effect

To further identify active species in the three oxidation systems, a series of scavengers (EtOH, TBA) was employed to capture the radicals responsible for the degradation reactions. EtOH was used to scavenge both HO• (1.2–2.8 $\times 10^9$ M^{-1} s^{-1}) and $SO_4^{\bullet-}$ (.6–7.7 $\times 10^7$ M^{-1} s^{-1}) [11], while TBA was used as an HO• scavenger (6 $\times 10^8$ M^{-1} s^{-1}) [36–39]. In general, furfuryl alcohol (FFA), sodium azide (NaN_3) and TEMP are common scavengers of $^1O_2$ [40–42], but FFA and sodium azide can be excessively consumed in persulfate-based electron-transfer processes, leading to an exaggerated contribution of singlet oxygenation in a nonradical system. Therefore, TEMP was selected as the $^1O_2$ quencher in this study [43]. EtOH and TBA showed negligible effects on SMX degradation in the systems with PMS alone (Fig. 3a) and ND/PMS (Fig. 3b), indicating that nonradicals might be the major pathway for SMX decomposition in the ND/PMS system. As shown in Fig. 3(b and d), the rate of SMX removal decreased significantly after TEMP was added, indicating that $^1O_2$ played an important role in the ND/PMS system. Similarly, these quenchers (EtOH, TBA and TEMP) were applied in the CNT/PMS system. EtOH more strongly inhibited the CNT/PMS system (Fig. 3d), while the effects of TBA and TEMP were insignificant. The results suggest that $SO_4^{\bullet-}$ is the ROS responsible for SMX oxidation in the CNT/PMS system (Fig. 3(c-d)). Moreover, to further explore the mechanism in the CNT/PMS system, we used benzoic acid (BA) to assess the contribution of radicals because BA can be oxidized by $SO_4^{\bullet-}$ through hydroxylation and Kolbe-type decarboxylation mechanisms and is immune to nonradical oxidation [44,45]. As shown in Fig. S3, the CNT/PMS system effectively decomposed BA with negligible adsorption on the CNT, confirming that $SO_4^{\bullet-}$ was generated in the CNT/PMS system.

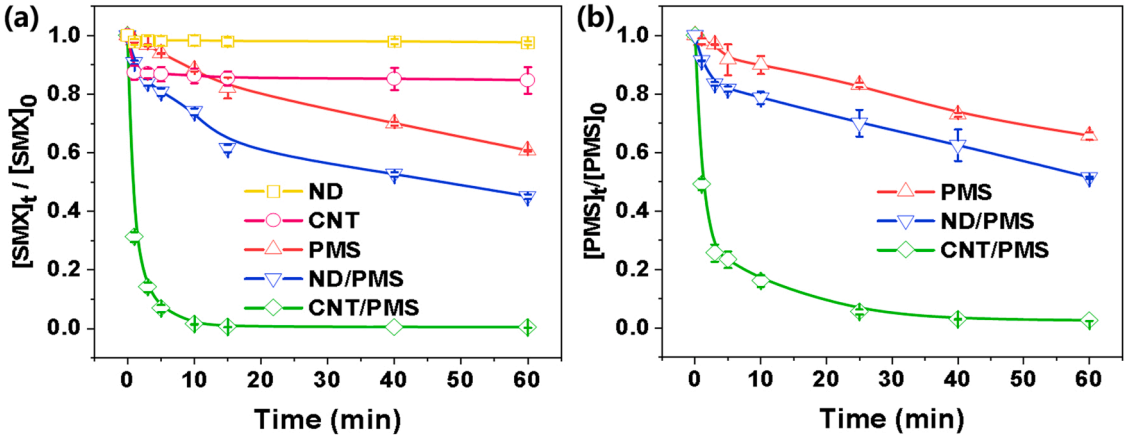

Fig. 1. Removal efficiency of SMX (a) and consumption rates of PMS (b) in ND and CNT adsorption and the three oxidation systems. Experimental conditions: $[SMX]_0 = 0.15$ mM; $[PMS]_0 = 0.5$ mM; pH = 7.0; [phosphate buffer] = 10 mM; $[catalyst]_0 = 0.1$ g L^{-1}; temperature= 25 ± 2 °C.

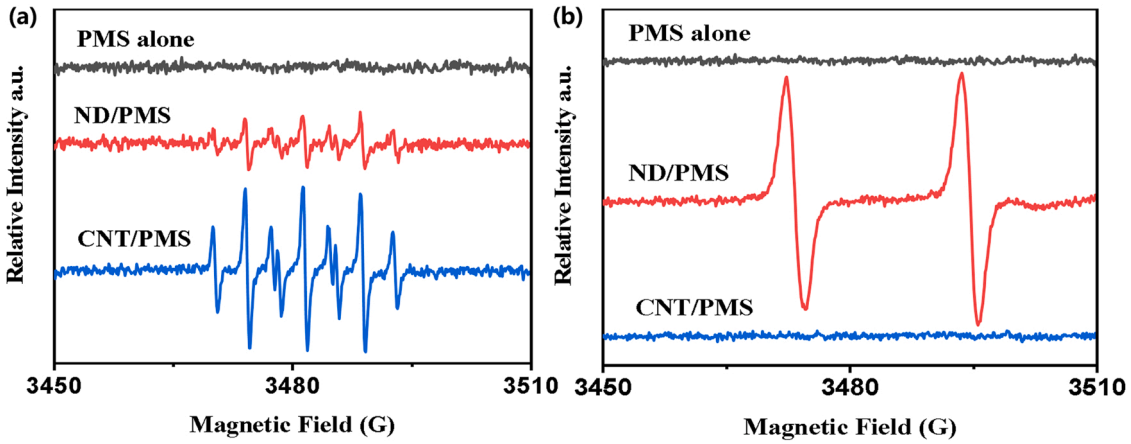

Fig. 2. EPR spectra obtained by spin trapping with the addition of DMPO (a) and TEMP (b) in the three oxidation systems. Experimental conditions: [PMS]= 0.5 mM; [DMPO]= 20 mM; [TEMP]= 20 mM; catalyst dosage= 0.1 g L^{-1}; pH= 7; [phosphate buffer]= 10 mM; temperature= 25 ± 2 °C.

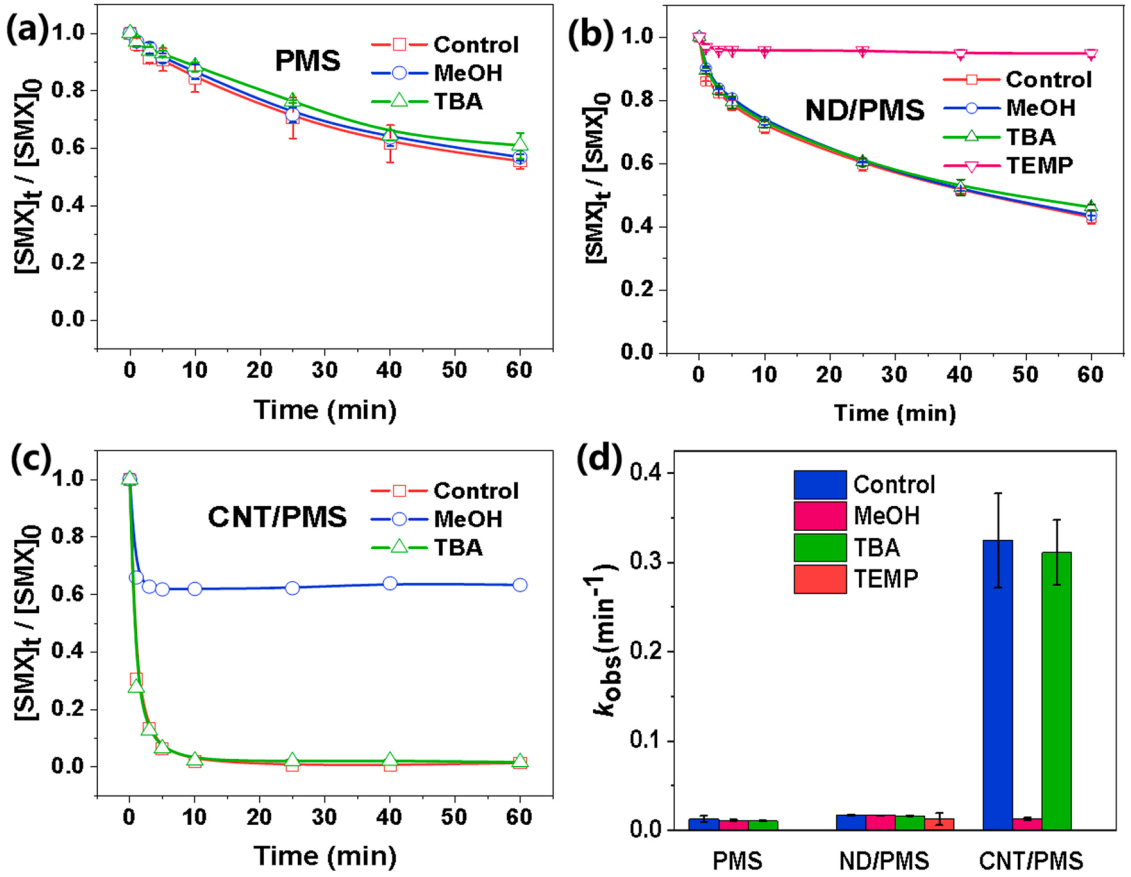

Fig. 3. Effect of alcohol scavengers on the system with only PMS (a), the ND/PMS system (b) and the CNT/PMS system (c); and k_{obs} (d). Experimental conditions: $[SMX]_0$ = 0.15 mM; [PMS]= 0.5 mM; [MeOH]/[PMS]= 500; [TBA]/[PMS]= 500; pH= 7.0; [phosphate buffer]= 10 mM; catalyst dose= 0.1 g L^{-1}; temperature= 25 ± 2 °C.

Moreover, open-circuit potential experiments were performed to evaluate the electron-transfer process [46]. As shown in Fig. S4, when PMS was added 100 s after the reaction, the potential of the CNT increased rapidly and gradually reached an equilibrium value of 0.75 V. Then, the equilibrium potential began to decline after the addition of SMX to the PMS solution. This phenomenon indicates that the CNT/PMS system involves an electron-transfer process. However, the changes in potential were not obvious in the PMS-alone and ND/PMS oxidation systems, indicating that the role of the electron-transfer process was insignificant in these two systems.

Based on the above discussion, SMX could be degraded via direct oxidation of PMS. Moreover, the main ROS and mechanism of the CNT/PMS system were $SO_4^{\bullet-}$ and nonradical electron transfer, while ND/PMS involved singlet oxygenation.

3.3. *Effect of water quality*

Protons, inorganic anions and NOM are common substances in

natural water and may disturb organic removal during oxidation processes. Therefore, anti-interference is a crucial parameter for evaluating application prospects in real water. Solution pH can affect the types of PMS formed (H_2SO_5, HSO_5^- and SO_5^{2-}, Text S3 and Fig. S5) [10]. As shown in Fig. 4a, the kinetic constants (~0.0040 min^{-1}) of PMS alone were stable in acid solution (initial pH $\leq$ 5), whereas the constants increased from 0.0043 min^{-1} (pH = 5) to 0.0092 min^{-1} (pH = 9) under alkaline conditions. The reason is that PMS transforms from HSO_5^- into SO_5^{2-}, in which the deprotonated species (SO_5^{2-}) nucleophilically attacks the distal O of the protonated species (HSO_5^-) to obtain a trioxide intermediate HSO_6^-, thereby increasing the SMX degradation activity under alkaline conditions [3].

In the ND/PMS process, when the pH was increased from 3 to 9, the rate of SMX removal gradually increased from 31.8% to 61.0% at 60 min (Fig. S6b), and the corresponding k_{obs} value increased from 0.008 min^{-1} to 0.027 min^{-1} (Fig. 4a) due to the favorable generation of $^1O_2$ under alkaline conditions [47]. However, the k_{obs} value increased by approximately 18-fold in the CNT/PMS system when the pH was increased from 3 (0.017 min^{-1}) to 7 (0.301 min^{-1}), and then, k_{obs} decreased to 0.087 min^{-1} as the pH was adjusted to 9 (Fig. 4a). This phenomenon can be explained as follows: (i) The main ROS in the CNT/PMS system were $SO_4^{\bullet-}$, CNT-PMS* complexes and PMS, which are likely to react with nucleophilic compounds, such as protons, pyrimidine compounds, and sulfonamides [3]. (ii) The nucleophilic interaction between $SO_4^{\bullet-}$/complexes and protons weakened, while the reaction between $SO_4^{\bullet-}$/complexes and SMX strengthened as the pH increased from 3 to 7, resulting in an enhanced rate of SMX removal. (iii) The rate of SMX removal decreased when the pH was adjusted to 9. This result is possibly due to the increased electrostatic repulsion between SO_5^{2-} and the catalyst surface, which led to decreased generation of $SO_4^{\bullet-}$.

The influences of humic acid (HA), HCO_3^- and Cl^- on the three oxidation systems were also studied (Fig. 4(b-d)). Inorganic anions (HCO_3^- and Cl^-) and NOM (HA) did not significantly affect the direct oxidation of SMX in the PMS-alone system. It has been reported that Cl^- can be activated into HOCl and Cl_2 in the presence of PMS (Eqs. 1 and 2) [48,49], but the removal rate was stable even in the presence of Cl^- in solution. This stability was because of the neutralization of active chlorines and direct oxidation of PMS: the generation of active chlorine species (HOCl and Cl_2) could accelerate the oxidation of SMX, but it would consume abundant PMS, leading to insufficient direct oxidation of PMS. The addition of HCO_3^-, HA, and Cl^- ions had almost no effect on the ND/PMS system because this system involves a $^1O_2$-dominated nonradical process that strongly resists interference [30]. Moreover, the effect of Cl^- was insignificant, suggesting that the competitive reactions of Cl^- with $SO_4^{\bullet-}$ were negligible because chlorine radicals (Eq. 3) can oxidize SMX directly, exhibiting a role similar to that of $SO_4^{\bullet-}$ in SMX degradation [47]. Moreover, HA had a certain effect on the degradation of SMX in the CNT/PMS system. It has been reported that $SO_4^{\bullet-}$ can be quenched by NOM (Eq. 4) [47]. Thus, the presence of NOM could decrease the amount of $SO_4^{\bullet-}$ required for the degradation of SMX. However, HCO_3^- had a significant effect on SMX degradation in the CNT/PMS system. It is reported that HCO_3^- can react with $SO_4^{\bullet-}$ to generate $CO_3^{\bullet-}$ (Eq. 5), which has a lower redox potential (E^0 = 1.63 V) than $SO_4^{\bullet-}$ (E^0 = 3.1 V), resulting in a significant inhibitory effect on the degradation of SMX [50,51].

$$HSO_5^- + Cl^- \rightarrow HOCl + SO_4^{2-} \quad (1)$$

$$HSO_5^- + 2Cl^- + H^+ \rightarrow Cl_2 + SO_4^{2-} + H_2O \quad (2)$$

$$Cl^{\cdot} + SO_4^{\cdot-} \rightarrow Cl^{\cdot} + SO_4^{2-} \quad (3)$$

$$NOM + SO_4^{\cdot-} \rightarrow NOM^{\cdot} + SO_4^{2-} \quad (4)$$

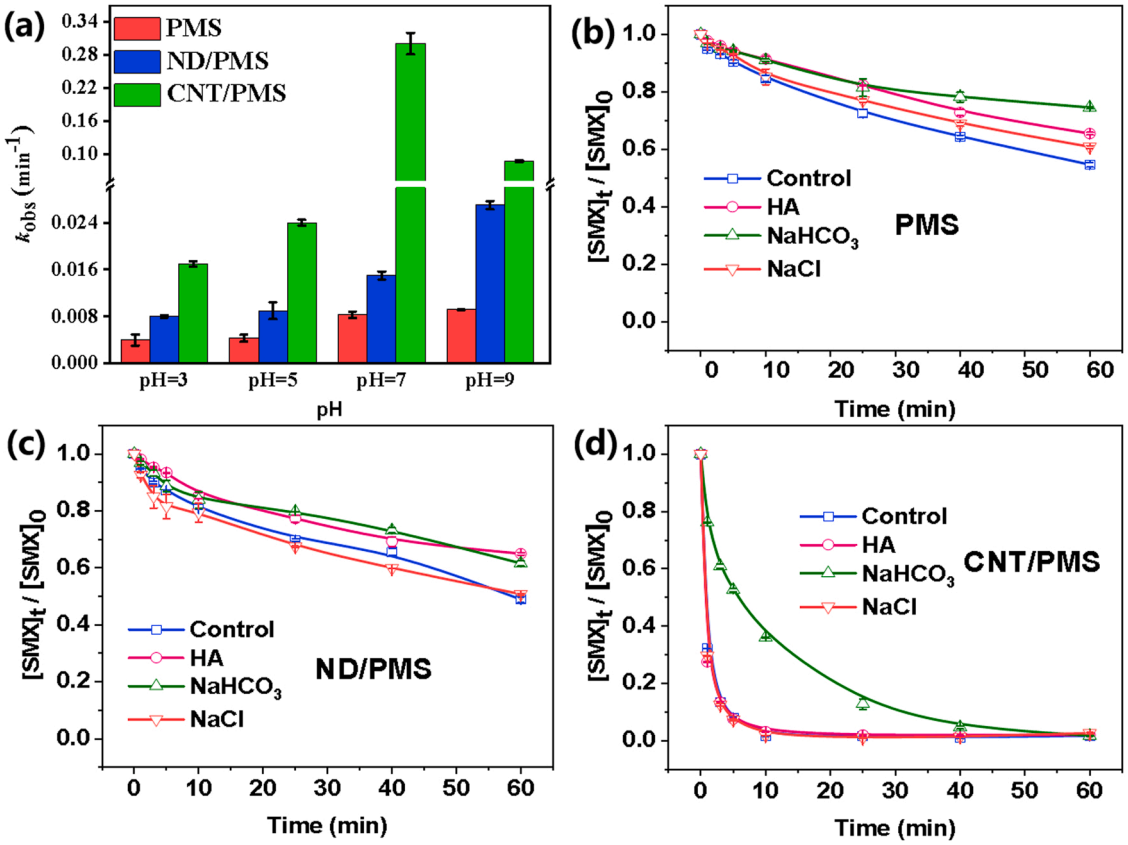

Fig. 4. (a) k_{obs} of SMX in different systems at pH= 3, 5, 7, and 9; (b) Effect of the common water quality constituents HA, HCO_3^-, and Cl^- in the PMS system (b), ND/PMS system (c) and CNT/PMS system (d). Experimental conditions: $[SMX]_0$ = 0.15 mM; [PMS]= 0.5 mM; pH= 7; [phosphate buffer]= 10 mM; [HA]= 10 mg L^{-1}; [$NaHCO_3$]= 10 mM; [NaCl]= 10 mM; catalyst dose= 0.1 g L^{-1}; temperature= 25 ± 2 °C.

$$HCO_3^- + SO_4^{\bullet-} \rightarrow CO_3^{\bullet-} + SO_4^{2-} + H^+ \quad (5)$$

The applications of three oxidation systems were researched in real water, including river and tap water. As shown in Fig. S7, the three systems still exhibited excellent performance in actual water, indicating that these systems have strong resistance to various water matrixes. Among the three compared oxidation systems, the CNT/PMS system is promising and highly efficient in eliminating antibiotics in practical water remediation applications.

3.4. Differences in the activation mechanisms of CNT and ND

According to the above experimental results, it can be concluded that both CNT and NDs can effectively activate PMS to degrade SMX. However, the main active species were different in the CNT/PMS ($SO_4^{\bullet-}$ and CNT-PMS* complexes) and ND/PMS ($^1O_2$) systems, which might be due to their nanostructures. CNT are composed of sp^2-conjugated carbon atoms, while ND has unique sp^3 hybridization characteristics in tetrahedral components. Therefore, the degradation of SMX by PMS activation occurs by different mechanisms. The reason for the different mechanisms is that the defects on CNT are important active sites that act as conductive carriers to facilitate the transfer of electrons, dominated by a potential difference from the highest occupied molecular orbital (HOMO) of SMX to the lowest unoccupied molecular orbital (LUMO) of the PMS molecule, providing an ideal active center for the electron transfer mechanism [27]. The ketone group of the CNT has a single pair of electrons, which tends to contribute an electron to PMS to form $SO_4^{\bullet-}$ for the degradation of SMX [29,52,53]. The main structure of the sp^3-hybridized system would be maintained if ND was annealed at medium and low temperatures ($\leq$ 900 ℃), and carbonyl groups on the ND surface contributed greatly to the activation of PMS to produce singlet oxygen [30,31]. Electrons can be transferred from the nucleophilic PMS (as an electron donor) to the electrophilic C═O group (as an electron acceptor). When an electron is released from PMS, a corresponding PMS anion radical ($SO_5^{\cdot-}$) is produced, resulting in the production of one $S_2O_8^{2-}$ or two SO_4^{2-} ions and a $^1O_2$ molecule [31].

3.5. Degradation pathway and evaluation of SMX toxicity

Toxicity is an important factor in measuring the success of water pollutant degradation. The activation of PMS on CNT and ND generated different active species, resulting in various intermediates during SMX oxidation. To evaluate the toxicity difference of the CNT/PMS/SMX and ND/PMS/SMX products, toxicity analysis of these products was conducted. The bacteriostatic effect of SMX on cell reproduction is derived from the sulfanilamide toxicophore, which induces competitive enzyme inhibition and metabolic interference due to its similar molecular structure to that of *p*-aminobenzoic acid (an important component involved in natural intracellular folic acid synthesis of bacteria) [54]. When testing the three oxidation systems of SMX and its transformation products (TPs) on green algae, the toxicity was observed to be significantly reduced after the three processes that used green algae as a receptor. As shown in Fig. 5, the SMX solution (0.15 mM) significantly inhibited algae growth. Compared with those of the blank control group, the OD and chlorophyll content of Chlorella were both reduced after the addition of SMX into solution, suggesting that SMX is toxic to green algae. Fortunately, the two parameters (OD and chlorophyll content) increased after the three oxidation systems were processed in the original SMX solution, indicating that the toxicity was lower after the three treatments. Notably, the OD and chlorophyll content both surpassed those of the blank group after oxidation with the CNT/PMS system, indicating that the growth of Chlorella was promoted rather than inhibited. This result occurred because the byproducts in the CNT/PMS system may have stimulated an increase in Chlorella cells, which is conducive to chlorophyll synthesis and promotes the growth of Chlorella. In addition, the degradation of SMX provides carbon and nitrogen sources for the growth of Chlorella.

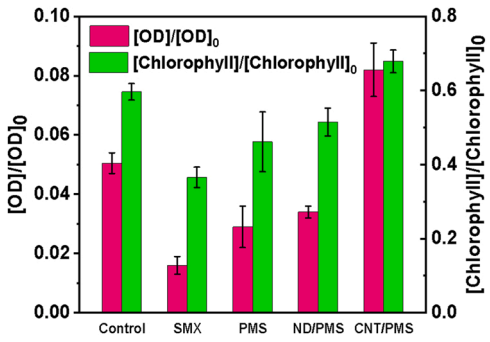

Fig. 5. The photodensity and chlorophyll content of the SMX solution and SMX solution degraded in the presence of Chlorella with the three oxidation systems. Experimental conditions: $[SMX]_0$ = 0.15 mM; [PMS]= 0.5 mM; catalyst dose= 0.1 g L^{-1}; pH= 7; temperature= 25 ± 2 °C.

The difference in toxicity of the three systems may be caused by their intermediates. Therefore, the intermediates were analyzed to investigate the degradation pathways of SMX and verify the mechanisms. A total of eight SMX nitrogen oxidation products were detected by ESI-TOF-MS (Table S4), and their molecular structures could be derived by accurate mass and fragment ions (Fig. S8-10). The electron density of each atom in the SMX structure was calculated by DFT (Fig. S11). An atom with a higher electron density in the functional group appears more blue. In contrast, an atom in an electron-deficient functional group appears red. The amino group (-NH_2) on the benzene ring in the SMX structure is an electron-rich functional group that is easily attacked by electrophilic ROS, which appears as blue in the DFT results. Hence, the possible degradation pathways of SMX in the three systems were proposed based on the information of intermediates, as shown in Fig. 6.

The comparatively high redox potential of PMS enables its direct, thermodynamically feasible oxidation with many organics. The electron-rich groups of SMX, such as phenols, anilines and alkenes, are generally vulnerable to electrophilic attack. The aniline group of SMX can eventually be oxidized into a nitro group (TP283, NO_2-SMX) by PMS, and the detailed pathways can be described as SMX →TP269 → TP267 →TP283, as observed in other oxidation processes, such as those with ferrate and chlorine dioxide [55]. However, this process did not cleave the N-S or C-S bonds of SMX to create smaller molecular compounds due to the limited oxidation of PMS.

$^1O_2$ is a highly selective oxidant that reacts almost exclusively with unsaturated organics via electrophilic addition and electron abstraction. In addition to the pathway of direct PMS oxidation, the ND/PMS system (singlet oxygenation) reacts via another similar pathway, that of SMX oxidation. The aniline group of SMX can be oxidized into a nitroso group (NO-SMX, TP267) followed by the subsequent cleavage of the N-S and C-S bonds for further oxidation [12]. Specifically, the cleavage of the N-S bond leads to the reduction of the sulfonyl group (-SO_2NH-) to a sulfinic acid group (-SO_2H) due to the electron-withdrawing effect of the sulfonamide moiety at the *para* position [56]. Subsequently, the C-S bond is broken through hydrolysis of the sulfinic acid group (-SO_2H) and converted into nitrosobenzene (TP107). The nitrosobenzene is then further oxidized into nitrobenzene (TP123).

$SO_4^{\bullet-}$ is a reactive electrophilic compound that reacts highly aggressively with electron-rich functional groups, undergoing reactions that include radical adduct formation, hydrogen atom abstraction and single electron transfer. This behavior causes $SO_4^{\bullet-}$ to exhibit superior oxidation on the aniline and thiazole ring amino groups of SMX. Apart from the pathways of nitrification of amino groups and the cleavage of N-S bonds, the unique reaction pathway (radical adduct formation) of $SO_4^{\bullet-}$ involves sulfonation of the sulfinic acid group (SMX → TP173 and TP283→ TP203), which differs from that of singlet oxygenation (TP267→ TP171).

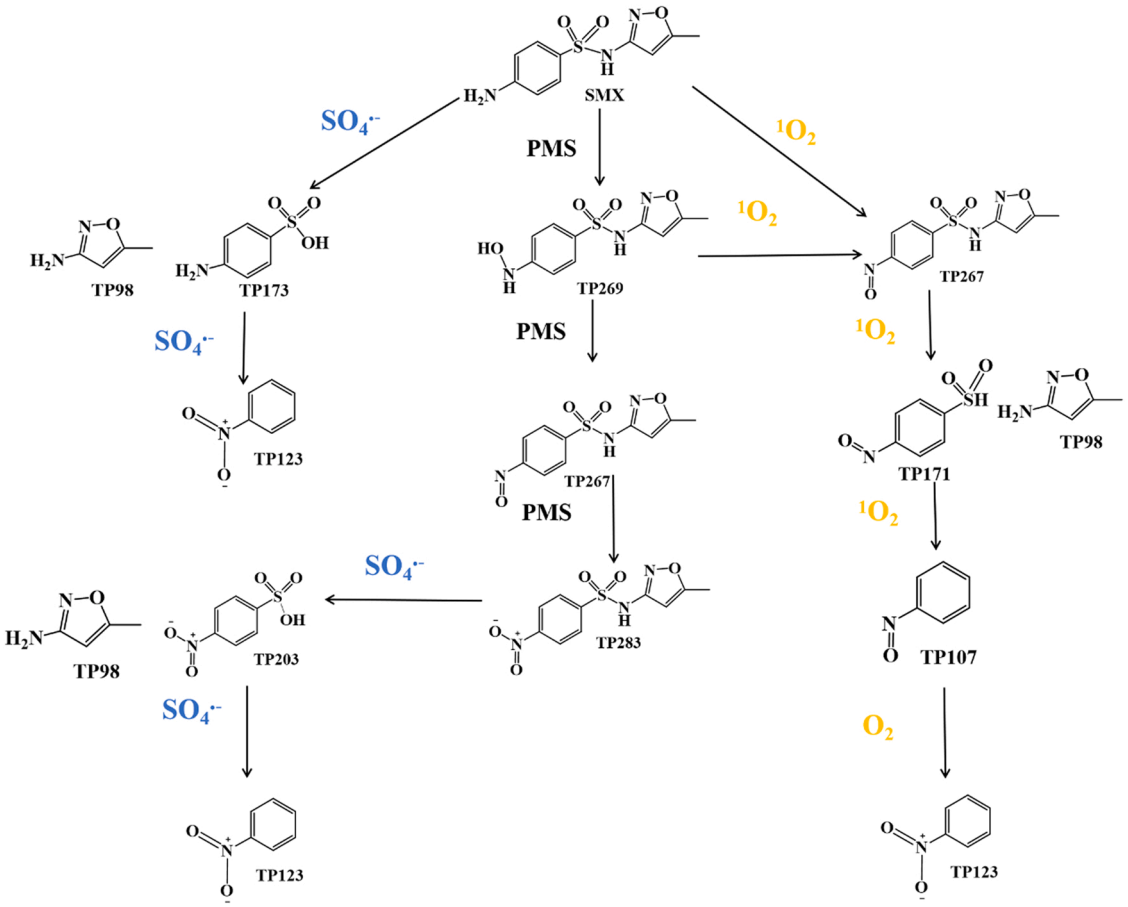

Fig. 6. Proposed reaction pathways for SMX degradation by the CNT/PMS system ($SO_4^{\cdot-}$ pathway), ND/PMS system ($^1O_2$ pathway) and PMS-alone system (PMS direct oxidation pathway).

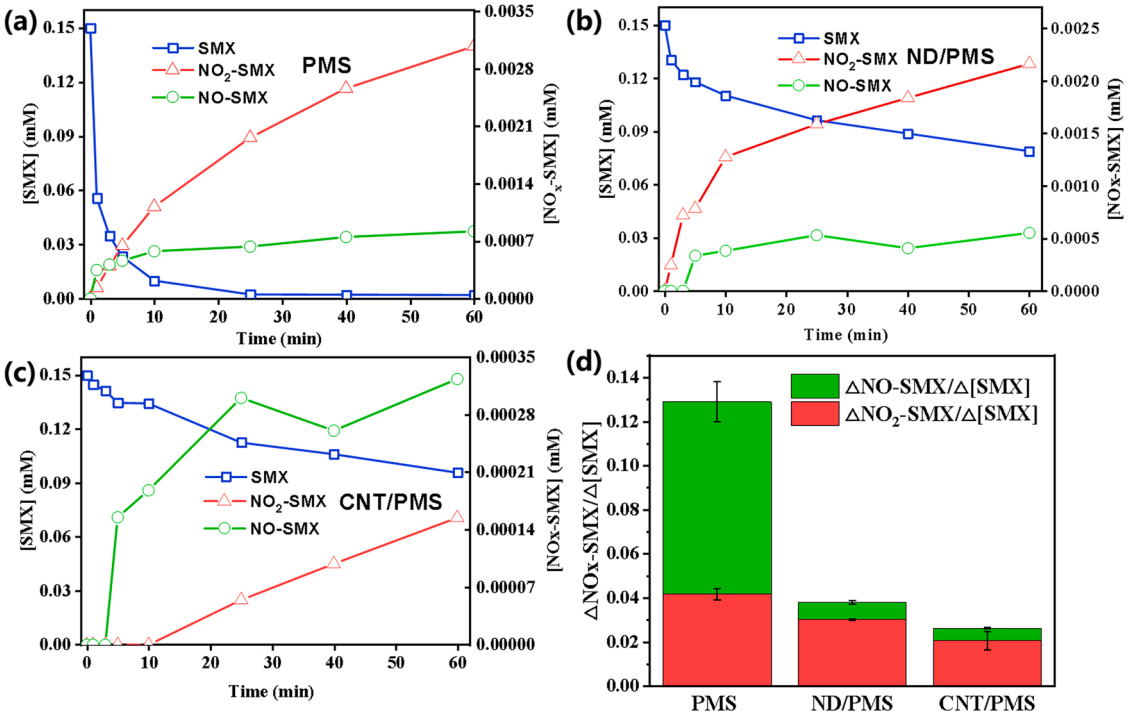

Fig. 7. Quantitative analysis of SMX consumption and NO_X-SMX products for the PMS system (a), ND/PMS system (b) and CNT/PMS system (c); [NOx-SMX]/△[SMX] in three oxidation systems (d). Experimental conditions: $[SMX]_0$ = 0.15 mM; [PMS]= 0.5 mM; pH= 7; [phosphate buffer]= 10 mM; catalyst dose = 0.1 g L^{-1}; temperature= 25 ± 2 °C.

In summary, the nitration of amino acids is the common pathway for the three oxidation processes. However, the three systems also undergo their own unique reactions when degrading SMX. In the system with PMS alone, SMX can undergo oxidation of its amino groups to nitroso and nitro groups without the cleavage of the N-S or C-S bonds. In the ND/PMS system, the sulfonyl group (-SO_2NH-) of SMX can be reduced to a sulfinic acid group (-SO_2H) by N-S bond cleavage, but the sulfinic acid group is not further oxidized into a sulfonic acid group. Fortunately, the sulfonation of SMX was achieved in the CNT/PMS system via cleavage of the N-S bond and radical addition.

Although SMX can be oxidized in the three systems, many nitroso products were produced in this study, suggesting that the toxicity of SMX was not completely removed and that the resulting solution was still toxic to the environment. Hence, the nitroso- and nitro-compounds were qualitatively and quantitatively analyzed by UPLC-TOF-MS. The concentrations of SMX and its nitroso-product (NO-SMX) and nitro-product (NO_2-SMX) are shown in Fig. 7(a-c) at different reaction times. The concentrations of the nitroso-product were higher than those of the nitro-product both in the CNT/PMS and ND/PMS systems, while the opposite was true in with PMS alone. The reason for this discrepancy is that PMS exhibits a mild oxidation capacity, resulting in the incomplete oxidation of amino groups. To further explore the mechanism of SMX degradation, four parameters, Δ[NO_X-SMX], Δ[NO-SMX] and Δ[NO_2-SMX], and Δ[SMX], were used to semiquantitatively evaluate the toxicity of water. Δ[NO_X-SMX] represents the total production of nitroso- and nitro-products (sum of Δ[NO-SMX] and Δ[NO_2-SMX]), and the expression (Δ[NO_X-SMX]/Δ[SMX]) represents the nitrification conversion rate of SMX because the nitro- and nitroso-products in the structures of NO_2-SMX and NO-SMX, respectively, are more toxic to the environment than SMX. As shown in Fig. 7d, the order of Δ[NO_X-SMX]/Δ[SMX] for the three oxidation systems was PMS alone > ND/PMS > CNT/PMS. These results indicate that the direct PMS oxidation of SMX produces more NO_X-SMX products than the two nanocarbon/PMS systems. The hope is that the production of NO_2-SMX and NO-SMX is reduced by water treatment; therefore, in the water treatment of sulfonamide antibiotics by persulfate advanced oxidation, the oxidation mode with $SO_4^{\bullet-}$ and electron transfer is superior to that with $^1O_2$ and PMS direct oxidation, and SMX degradation by oxidation can reduce the production of NO_2-SMX or NO-SMX, byproducts that are more toxic to the environment than SMX. However, SMX could not be completely removed via the ND/PMS system, and the residual SMX potentially remained toxic. Based on the results of the toxicological experiments, the CNT/PMS system is more conducive to the degradation of SMX in engineering practice.

4. Conclusions

In summary, we compared the differences in the activation mechanism of PMS on two nanocarbon materials (CNT and ND) and the degradation pathways of SMX in the corresponding CNT/PMS and ND/PMS systems. EPR, chemical quenching and open-circuit potential experiments showed that the CNT/PMS system involved sulfate radical oxidation and electron-transfer processes, while the ND/PMS system could produce singlet oxygen. Kinetic experiments showed that the CNT/PMS system was the most effective for SMX degradation both in removal and oxidation rates, and it still exhibited superior performance in actual water samples. Moreover, the product and toxicity analyses well explained the degradation and detoxification pathways of SMX during the CNT/PMS and ND/PMS processes. This study provides new insight into the removal of antibiotics via the activation of PMS on carbon materials for advanced oxidation technology. More importantly, the CNT/PMS system provides a promising technology for the control and toxicity reduction of antibiotics in actual wastewater.

CRediT authorship contribution statement

Yanhua Peng: Methodology, Investigation, Data curation, Writing – original draft. **Guansheng Xie:** Investigation, Methodology, Data curation. **Penghui Shao:** Formal analysis, Validation, Visualization, Writing – review & editing. **Wei Ren:** Visualization, Writing – review & editing. **Mengling Li:** Investigation, Formal analysis. **Yufeng Hu:** Theoretical calculation, Investigation, Formal analysis. **Liming Yang:** Methodology, Formal analysis. **Hui Shi:** Methodology, Formal analysis. **Xubiao Luo:** Methodology, Formal analysis, Supervision.

Declaration of Competing Interest

The authors declare that they have no known competing financial interests or personal relationships that could have appeared to influence the work reported in this paper.

Acknowledgments

This study was financially supported by the National Natural Science Foundation of China (No. 51908270 and 52125002), the Natural Science Foundation of Jiangxi Province (No. 20212ACB213006), and the National Key Research and Development Program of China (No. 2019YFC1907900).

Appendix A. Supporting information

Supplementary data associated with this article can be found in the online version at doi:10.1016/j.apcatb.2022.121345.

References

[1] S. Fallah, H.R. Mamaghani, R. Yegani, N. Hajinajaf, B. Pourabbas, Use of graphene substrates for wastewater treatment of textile industries, Adv. Compos. Hybrid. Mater. 3 (2020) 187–193, https://doi.org/10.1007/s42114-020-00146-4.
[2] Y. Shao, H. Bai, H. Wang, G. Fei, L. Li, Y. Zhu, HBFP: a new repository for human body fluid proteome, Adv. Compos. Hybrid. Mater. 2021 (2021), https://doi.org/10.1007/s42114-021-00361-7.
[3] Y. Yang, G. Banerjee, G.W. Brudvig, J.H. Kim, J.J. Pignatello, Oxidation of organic compounds in water by unactivated peroxymonosulfate, Environ. Sci. Technol. 52 (2018) 5911–5919, https://doi.org/10.1021/acs.est.8b00735.
[4] K. Kummerer, Antibiotics in the aquatic environment–a review–part I, Chemosphere 75 (2009) 417–434, https://doi.org/10.1016/j.chemosphere.2008.11.086.
[5] Z. Deng, S. Sun, H. Li, D. Pan, R.R. Patil, Z. Guo, I. Seok, Modification of coconut shell-based activated carbon and purification of wastewater, Adv. Compos. Hybrid. Mater. 4 (2021) 65–73, https://doi.org/10.1007/s42114-021-00205-4.
[6] J. Ziemianska, E. Adamek, A. Sobczak, I. Lipska, A. Makowski, W. Baran, Physicochem. Probl. Miner. Process 45 (2010) 127–140.
[7] Q. Hu, J. Zhou, B. Qiu, Q. Wang, G. Song, Z. Guo, Synergistically improved methane production from anaerobic wastewater treatment by iron/polyaniline composite, Adv. Compos. Hybrid. Mater. 4 (2021) 265–273, https://doi.org/10.1007/s42114-021-00236-x.
[8] C. Lin, B. Liu, L. Pu, Y. Sun, Y. Xue, M. Chang, X. Li, X. Lu, R. Chen, J. Zhang, Photocatalytic oxidation removal of fluoride ion in wastewater by g-C3N4/TiO2 under simulated visible light, Adv. Compos. Hybrid. Mater. 4 (2021) 339–349, https://doi.org/10.1007/s42114-021-00228-x.
[9] C. Yin, C. Wang, Q. Hu, Selective removal of As(V) from wastewater with high efficiency by glycine-modified Fe/Zn-layered double hydroxides, Adv. Compos. Hybrid. Mater. 4 (2021) 360–370, https://doi.org/10.1007/s42114-021-00214-3.
[10] C. Guan, J. Jiang, S. Pang, J. Ma, X. Chen, T.-T. Lim, Nonradical transformation of sulfamethoxazole by carbon nanotube activated peroxydisulfate: kinetics, mechanism and product toxicity, Chem. Eng. J. 378 (2019), 122147, https://doi.org/10.1016/j.cej.2019.122147.
[11] Y. Shang, C. Chen, P. Zhang, Q. Yue, Y. Li, B. Gao, X. Xu, Quantitative proteome reveals variation in the condition factor of sea urchin strongylocentrotus nudus during the fishing season using an iTRAQ-based approach, Chem. Eng. J. 375 (2019), https://doi.org/10.1016/j.cej.2019.122004.
[12] R. Yin, W. Guo, H. Wang, J. Du, Q. Wu, J.-S. Chang, N. Ren, Porcine insulin receptor substrate 2: molecular cloning, tissues distribution, and functions in hepatocyte and aortic endothelial cells, Chem. Eng. J. 357 (2019) 589–599, https://doi.org/10.1016/j.cej.2018.09.184.
[13] A. Vijeata, G.R. Chaudhary, A. Umar, S. Chaudhary, Eng. Sci. (2021), https://doi.org/10.30919/es8e512.

[14] H. Han, H. Sun, F. Lei, J. Huang, S. Lyu, B. Wu, M. Yang, C. Zhang, D. Li, Z. Zhang, D. Sun, Machine learning regression guided thermoelectric materials discovery – a review, ES Mater. Manuf. (2021), https://doi.org/10.30919/esmm5f523.
[15] M. Kumari, G.R. Chaudhary, S. Chaudhary, A. Umar, Identification and characterization of non-small cell lung cancer associated sialoglycoproteins, Eng. Sci. 248 (2021), 104336, https://doi.org/10.30919/es8d556.
[16] X. Duan, H. Sun, J. Kang, Y. Wang, S. Indrawirawan, S. Wang, Insights into heterogeneous catalysis of persulfate activation on dimensional-structured nanocarbons, ACS Catal. 5 (2015) 4629–4636, https://doi.org/10.1021/acscatal.5b00774.
[17] H. Lee, H.I. Kim, S. Weon, W. Choi, Y.S. Hwang, J. Seo, C. Lee, J.H. Kim, Activation of persulfates by graphitized nanodiamonds for removal of organic compounds, Environ. Sci. Technol. 50 (2016) 10134–10142, https://doi.org/10.1021/acs.est.6b02079.
[18] C.R. Martin, P. Kohli, The emerging field of nanotube biotechnology, Nat. Rev. Drug Disco 2 (2003) 29–37, https://doi.org/10.1038/nrd988.
[19] M. Farahmandian, M. Saidi, S. Fazlinejad, Adv. Compos. Hybrid. Mater. (2021), https://doi.org/10.1007/s42114-021-00220-5.
[20] M.J. Islam, M.J. Rahman, T. Mieno, Advanced biological sequential treatment of mature landfill leachate using aerobic activated sludge SBR and fungal bioreactor, Adv. Compos. Hybrid. Mater. 3 (2020) 285–293, https://doi.org/10.1007/s42114-020-00160-6.
[21] H.M. Khater, A.M. El-Nagar, Preparation of sustainable of eco-friendly MWCNT-geopolymer composites with superior sulfate resistance, Adv. Compos. Hybrid. Mater. 3 (2020) 375–389, https://doi.org/10.1007/s42114-020-00170-4.
[22] X. Luo, G. Yang, D.W. Schubert, Adv. Compos. Hybrid. Mater. (2021), https://doi.org/10.1007/s42114-021-00332-y.
[23] K. Qu, Z. Sun, C. Shi, W. Wang, L. Xiao, J. Tian, Z. Huang, Z. Guo, Dual-acting cellulose nanocomposites filled with carbon nanotubes and zeolitic imidazolate framework-67 (ZIF-67)–derived polyhedral porous Co3O4 for symmetric supercapacitors, Adv. Compos. Hybrid. Mater. 4 (2021) 670–683, https://doi.org/10.1007/s42114-021-00293-2.
[24] Z. Wang, X. Li, L. Wang, Y. Li, J. Qin, P. Xie, Y. Qu, K. Sun, R. Fan, Flexible multi-walled carbon nanotubes/polydimethylsiloxane membranous composites toward high-permittivity performance, Adv. Compos. Hybrid. Mater. 3 (2020) 1–7, https://doi.org/10.1007/s42114-020-00144-6.
[25] N. Wu, B. Zhao, J. Liu, Y. Li, Y. Chen, L. Chen, M. Wang, Z. Guo, Exposure of zebra mussels to radial extracorporeal shock waves: implications for treatment of fracture nonunions, Adv. Compos. Hybrid. Mater. 4 (2021) 707–715, https://doi.org/10.1007/s42114-021-00307-z.
[26] W. Ren, L. Xiong, G. Nie, H. Zhang, X. Duan, S. Wang, Insights into the electron-transfer regime of peroxydisulfate activation on carbon nanotubes: the role of oxygen functional groups, Environ. Sci. Technol. 54 (2020) 1267–1275, https://doi.org/10.1021/acs.est.9b06208.
[27] P. Shao, S. Yu, X. Duan, L. Yang, H. Shi, L. Ding, J. Tian, L. Yang, X. Luo, S. Wang, Potential difference driving electron transfer via defective carbon nanotubes toward selective oxidation of organic micropollutants, Environ. Sci. Technol. 54 (2020) 8464–8472, https://doi.org/10.1021/acs.est.0c02645.
[28] V.V. Danilenko, On the history of the discovery of nanodiamond synthesis, Springer, 2004, pp. 595–599.
[29] X. Duan, C. Su, L. Zhou, H. Sun, A. Suvorova, T. Odedairo, Z. Zhu, Z. Shao, S. Wang, Surface controlled generation of reactive radicals from persulfate by carbocatalysis on nanodiamonds, Appl. Catal. B: Environ. 194 (2016) 7–15, https://doi.org/10.1016/j.apcatb.2016.04.043.
[30] P. Shao, Y. Jing, X. Duan, H. Lin, L. Yang, W. Ren, F. Deng, B. Li, X. Luo, S. Wang, Revisiting the graphitized nanodiamond-mediated activation of peroxymonosulfate: singlet oxygenation versus electron transfer, Environ. Sci. Technol. 55 (2021) 16078–16087, https://doi.org/10.1021/acs.est.1c02042.
[31] P. Shao, J. Tian, F. Yang, X. Duan, S. Gao, W. Shi, X. Luo, F. Cui, S. Luo, S. Wang, Adv. Funct. Mater. 28 (2018), https://doi.org/10.1002/adfm.201705295.
[32] Y. Zhang, Z. Xiong, L. Yang, Z. Ren, P. Shao, H. Shi, X. Xiao, S.G. Pavlostathis, L. Fang, X. Luo, Water Res 166 (2019), 115076, https://doi.org/10.1016/j.watres.2019.115076.
[33] S.V. Verstraeten, S. Lucangioli, M. Galleano, ESR characterization of thallium(III)-mediated nitrones oxidation, Inorg. Chim. Acta 362 (2009) 2305–2310, https://doi.org/10.1016/j.ica.2008.10.013.
[34] J.R. Harbour, S.L. Issler, M.L. Hair, Singlet oxygen and spin trapping with nitrones, J. Am. Chem. Soc. 102 (1980) 7778–7779, https://doi.org/10.1021/ja00546a024.
[35] A. Lawrence, C.M. Jones, P. Wardman, M.J. Burkitt, Evidence for the role of a peroxidase compound I-type intermediate in the oxidation of glutathione, NADH, ascorbate, and dichlorofluorescin by cytochrome c/H2O2. Implications for oxidative stress during apoptosis, J. Biol. Chem. 278 (2003) 29410–29419, https://doi.org/10.1074/jbc.M300054200.
[36] H. Chen, Z. Zhang, M. Feng, W. Liu, W. Wang, Q. Yang, Y. Hu, Degradation of 2,4-dichlorophenoxyacetic acid in water by persulfate activated with FeS (mackinawite, Chem. Eng. J. 313 (2017) 498–507, https://doi.org/10.1016/j.cej.2016.12.075.
[37] C. Dong, J. Ji, B. Shen, M. Xing, J. Zhang, Enhancement of H2O2 decomposition by the co-catalytic effect of WS2 on the fenton reaction for the synchronous reduction of Cr(VI) and remediation of phenol, Environ. Sci. Technol. 52 (2018) 11297–11308, https://doi.org/10.1021/acs.est.8b02403.
[38] J. Zhang, J. Ma, H. Song, S. Sun, Z. Zhang, T. Yang, Organic contaminants degradation from the S(IV) autoxidation process catalyzed by ferrous-manganous ions: a noticeable Mn(III) oxidation process, Water Res 133 (2018) 227–235, https://doi.org/10.1016/j.watres.2018.01.039.
[39] X. Zhang, M. Feng, R. Qu, H. Liu, L. Wang, Z. Wang, Catalytic degradation of diethyl phthalate in aqueous solution by persulfate activated with nano-scaled magnetic CuFe 2 O 4 /MWCNTs, Chem. Eng. J. 301 (2016) 1–11, https://doi.org/10.1016/j.cej.2016.04.096.
[40] J. Moan, E. Wold, Detection of singlet oxygen production by ESR, Nature 279 (1979) 450–451, https://doi.org/10.1038/279450a0.
[41] B. Song, G. Wang, M. Tan, J. Yuan, A europium(III) complex as an efficient singlet oxygen luminescence probe, J. Am. Chem. Soc. 128 (2006) 13442–13450, https://doi.org/10.1021/ja062990f.
[42] Y. Zhou, J. Jiang, Y. Gao, J. Ma, S.Y. Pang, J. Li, X.T. Lu, L.P. Yuan, Activation of peroxymonosulfate by benzoquinone: a novel nonradical oxidation process, Environ. Sci. Technol. 49 (2015) 12941–12950, https://doi.org/10.1021/acs.est.5b03595.
[43] X. Cheng, H. Guo, Y. Zhang, G.V. Korshin, B. Yang, Insights into the mechanism of nonradical reactions of persulfate activated by carbon nanotubes: Activation performance and structure-function relationship, Water Res. 157 (2019) 406–414, https://doi.org/10.1016/j.watres.2019.03.096.
[44] V. Madhavan, H. Levanon, P. Neta, Decarboxylation by S. O 4 - radicals, Radiat. Res. 76 (1978) 15–22, https://doi.org/10.2307/3574923.
[45] H. Zemel, R.W. Fessenden, The mechanism of reaction of sulfate radical anion with some derivatives of benzoic acid, J. Phys. Chem. 82 (1978) 2670–2676, https://doi.org/10.1021/j100514a008.
[46] W. Ren, P. Zhou, G. Nie, C. Cheng, X. Duan, H. Zhang, S. Wang, Hydroxyl radical dominated elimination of plasticizers by peroxymonosulfate on metal-free boron: Kinetics and mechanisms, Water Res 186 (2020), 116361, https://doi.org/10.1016/j.watres.2020.116361.
[47] J. Lee, U. von Gunten, J.H. Kim, Persulfate-based advanced oxidation: critical assessment of opportunities and roadblocks, Environ. Sci. Technol. 54 (2020) 3064–3081, https://doi.org/10.1021/acs.est.9b07082.
[48] G.P. Anipsitakis, D.D. Dionysiou, M.A. Gonzalez, Cobalt-mediated activation of peroxymonosulfate and sulfate radical attack on phenolic compounds. implications of chloride ions, Environ. Sci. Technol. 40 (2006) 1000–1007, https://doi.org/10.1021/es050634b.
[49] T. Lei, R. Barzilay, T. Jaakkola, arXiv preprint arXiv:1606.04155, 2016. https://doi.org/abs/1606.04155.
[50] W. Ren, C. Cheng, P. Shao, X. Luo, H. Zhang, S. Wang, X. Duan, Origins of electron-transfer regime in persulfate-based nonradical oxidation processes, Environ. Sci. Technol. 56 (2022) 78–97, https://doi.org/10.1021/acs.est.1c05374.
[51] R. Zhang, P. Sun, T.H. Boyer, L. Zhao, C.H. Huang, Degradation of pharmaceuticals and metabolite in synthetic human urine by UV, UV/H2O2, and UV/PDS, Environ. Sci. Technol. 49 (2015) 3056–3066, https://doi.org/10.1021/es504799n.
[52] H. Sun, C. Kwan, A. Suvorova, H.M. Ang, M.O. Tadé, S. Wang, Catalytic oxidation of organic pollutants on pristine and surface nitrogen-modified carbon nanotubes with sulfate radicals, Appl. Catal. B Environ. 154–155 (2014) 134–141, https://doi.org/10.1016/j.apcatb.2014.02.012.
[53] H. Sun, S. Liu, G. Zhou, H.M. Ang, M.O. Tade, S. Wang, Reduced graphene oxide for catalytic oxidation of aqueous organic pollutants, ACS Appl. Mater. Interfaces 4 (2012) 5466–5471, https://doi.org/10.1021/am301372d.
[54] M. Majewsky, D. Wagner, M. Delay, S. Brase, V. Yargeau, H. Horn, Antibacterial activity of sulfamethoxazole transformation products (TPs): general relevance for sulfonamide TPs modified at the para position, Chem. Res Toxicol. 27 (2014) 1821–1828, https://doi.org/10.1021/tx500267x.
[55] W. Ben, Y. Shi, W. Li, Y. Zhang, Z. Qiang, Oxidation of sulfonamide antibiotics by chlorine dioxide in water: kinetics and reaction pathways, Chem. Eng. J. 327 (2017) 743–750, https://doi.org/10.1016/j.cej.2017.06.157.
[56] Y. Ji, Y. Fan, K. Liu, D. Kong, J. Lu, Thermo activated persulfate oxidation of antibiotic sulfamethoxazole and structurally related compounds, Water Res. 87 (2015) 1–9, https://doi.org/10.1016/j.watres.2015.09.005.